Sensor Response Mismatches and Lag Correction Techniques for Temperature-Salinity Profilers[1]

E. P. W. HORNE[2] AND J. M. TOOLE[3]

Woods Hole Oceanographic Institution, Woods Hole, MA 02543

(Manuscript received 1 January 1980, in final form 2 April 1980)

ABSTRACT

Salinity-temperature-depth profilers measure temperature directly but infer salinity from measurements of temperature, pressure and conductivity. Errors may therefore be introduced into the salinity data because of dissimilar response characteristics of the various sensors. This response mismatch usually manifests itself as the temperature signal lagging the conductivity signal in time. An error analysis demonstrates that amplitude underestimations of only 1% with a phase error of only 5° in the temperature data can result in a 20% overestimation of salinity variance. Techniques for removing the effects of sensor-response mismatches in the data are discussed and a new method is presented. The method involves the determination of correction filters for the data in physical space in terms of the response function of the sensors which is in frequency space. Thermohaline features on vertical scales smaller than 1 m appear resolvable in CTD data that are corrected with this technique.

1. Introduction

Several instruments have been developed in the past two decades that provide virtually continuous vertical profiles of temperature and salinity (Hamon and Brown, 1958; Brown, 1963; Gregg and Cox, 1971; Kroebel, 1973; Brown, 1974). Temperature is measured directly by these instruments. However, there is no sensor which measures salinity directly. Thus algorithms that require data from several sensors are employed to calculate salinity. These algorithms use temperature, conductivity, and pressure data with the dominant contribution to the calculated salinity coming from the temperature and conductivity. Since data from several sensors are required, the possibility exists that errors may be introduced in the calculated salinity data by the dissimilar response characteristics of the various sensors.

The major sensor response mismatch in these instruments is due to the temperature probe, whose signal lags behind the signal from the conductivity sensor in time. In Section 2 the characteristics of this response mismatch and the errors it introduces are discussed. Techniques for correcting the mismatch are reviewed in Section 3 and a new method for lag correction is presented. The analysis will be presented for the thermistor data from a WHOI/NBIS CTD (Brown, 1974; Millard *et al.*, 1980) but the error discussion and response-correction technique is applicable to other profiling instruments.

2. Error estimates due to sensor-response mismatches

a. Sensor responses

Profiling instruments generally sense temperature with a probe whose resistance varies with temperature. The temperature probe has a finite size and so disrupts the fluid as it profiles the water column. The oceanic temperature signal must diffuse through the fluid boundary layer set up about the probe as well as one or more protective coatings on the sensor (Lueck *et al.*, 1977). Finally the thermal mass of the sensor head must respond before the instrument records the temperature signal. The observed temperature data are thus a smoothed and distorted version of the actual temperature.

The observed temperature T_O, may be expressed as a convolution between the true temperature T_T, and the transfer or response function of the sensor f,

$$T_O(t) = f * T_T(t). \quad (1)$$

If the lowering rate is uniform, f is constant. In frequency space, the typical response characteristics of a temperature probe are decreasing amplitude response $R(\omega)$ and increasing phase lag $\theta(\omega)$ with in-

[1] Woods Hole Oceanographic Institution Contribution No. 4509.

[2] Present affiliation: Marine Ecology Laboratory, Bedford Institute of Oceanography, P.O. Box 1006, Dartmouth, N.S., Canada, B2Y 4A2.

[3] Present affiliation: National Research Council Research Associate at the Pacific Marine Environmental Laboratory, Seattle, WA 98105.

0022-3670/80/071122-09$06.25

creasing frequency ω, i.e.,

$$\hat{f} = R(\omega) \exp[i\theta(\omega)]. \quad (2)$$

The Fourier transform is denoted here by a caret. The response function of the fast-response thermistor on the WHOI/Brown CTD determined by Millard *et al.* (1980) is shown in Fig. 1.

The response of a conductivity cell is a function of the flushing rate of the cell, including the fluid boundary layers on the cell walls. Brown (1979, personal communication) estimates the flushing time for the square 0.3 m long conductivity cell on the CTD is ~0.03 s at typical lowering rates of 60–80 m min^{-1}. The CTD has a 30 Hz sampling rate, so each conductivity data point is virtually independent information. The response of the conductivity sensor becomes important only on vertical scales < 5 cm, which are not resolved by the CTD sampling scheme. The response time of the conductivity sensor is thus shorter than that of the temperature sensor. This sensor response mismatching has a severe impact on the calculated salinity.

b. *Salinity noise*

The effects of the sensor-response mismatch in physical space are shown schematically in Fig. 2 where data obtained from an instrument profiling across a step change in conductivity, temperature and salinity are plotted, following Dantzler (1974). The conductivity sensor responds rapidly across the step and, in this example, perfectly resolves the step in conductivity. The temperature sensor has a finite response time, and so, just below the step, the observed temperature is lower than the true temperature. The salinity, calculated with the observed

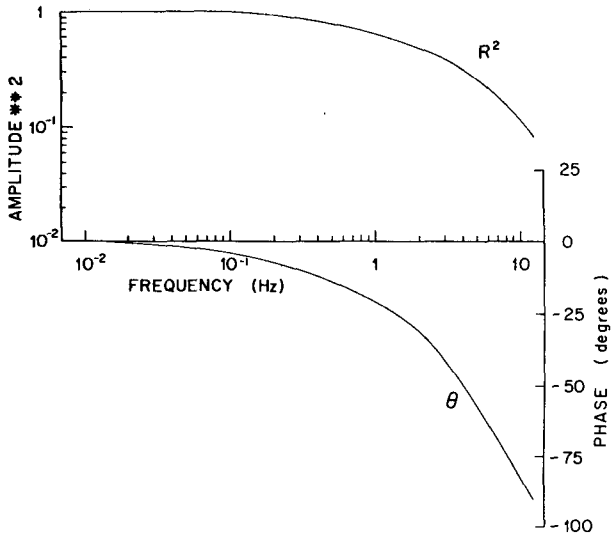

FIG. 1. The amplitude and phase response of the thermistor on the WHOI/Brown CTD.

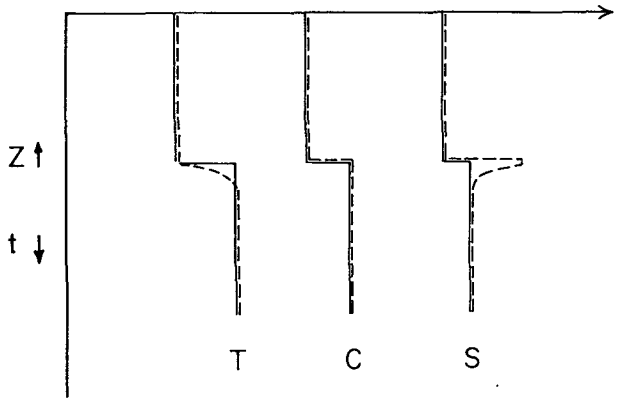

FIG. 2. Temperature, conductivity and salinity profiles across a small step (solid curve) and typical profiles obtained with a profiling instrument which has a temperature sensor which responds slower than its conductivity sensor (dashed line).

temperature and conductivity below the step, is larger than the true salinity as a result. A characteristic of the sensor-response mismatch in physical space is overshooting or spiking (Dantzler, 1974; Scarlet, 1975) of the calculated salinity when the temperature or conductivity changes rapidly.

The characteristics of the sensor mismatch in frequency space may be examined with a linearized form of the salinity algorithm.

$$dS = \left(\frac{\partial S}{\partial T}\right)dT + \left(\frac{\partial S}{\partial C}\right)dC + O(dP, dT^2, dC^2 \ldots), \quad (3)$$

where S is the salinity and C the conductivity. The salinity spectral energy density computed with the true temperature and observed temperature [given by Eq. (1)] are, respectively,

$$(\hat{S}_T\hat{S}_T^*) = (\hat{T}_T\hat{T}_T^*)\left\{\left(\frac{\partial S}{\partial T}\right)^2 + \left(\frac{\partial S}{\partial C}\right)^2 \frac{(\hat{C}\hat{C}^*)}{(\hat{T}_T\hat{T}_T^*)} + 2\left(\frac{\partial S}{\partial T}\right)\left(\frac{\partial S}{\partial C}\right)[(\hat{C}\hat{C}^*)(\hat{T}_T\hat{T}_T^*)^{-1}]^{1/2}\right\} \quad (4a)$$

$$(\hat{S}_O\hat{S}_O^*) = (\hat{T}_T\hat{T}_T^*)\left\{\left(\frac{\partial S}{\partial T}\right)^2 R^2 + \left(\frac{\partial S}{\partial C}\right)^2 \frac{(\hat{C}\hat{C}^*)}{(\hat{T}_T\hat{T}_T^*)} + 2\left(\frac{\partial S}{\partial T}\right)\left(\frac{\partial S}{\partial C}\right)[(\hat{C}\hat{C}^*)(\hat{T}_T\hat{T}_T^*)^{-1}R^2]^{1/2}\cos\theta\right\}. \quad (4b)$$

In the above, the spectral energy density of the true temperature and conductivity have been written as $(\hat{T}_T\hat{T}_T^*)$ and $(\hat{C}\hat{C}^*)$, where the asterisk superscript denotes the complex conjugate, while the amplitude response of the temperature sensor is given by R^2.

Similarly, the phase angle between the observed temperature and calculated salinity ϕ may be

written as

$$\phi = \tan^{-1}\left\{ \frac{\sin\theta}{\cos\theta + \left(\frac{\partial S}{\partial T}\right)\left(\frac{\partial S}{\partial C}\right)^{-1}[(\hat{T}_T\hat{T}_T^*)(\hat{C}\hat{C}^*)^{-1}R^2]^{1/2}} \right\}. \quad (5)$$

In deriving (4) and (5) it was assumed that the conductivity was perfectly coherent with the true and observed temperatures and in phase with the true temperature. The sense of the sensor-response mismatch is to overestimate the salinity variance if the temperature amplitude response is underestimated or if the temperature data are out of phase with the true temperature.

c. *Density noise*

The data from profiling instruments are often used to compute the vertical density profile or its gradient. The errors induced in the temperature and salinity data from the sensor response mismatch also have an effect on the density. The characteristics of this density signal may be estimated if a linear equation of state is assumed.

$$\rho = \rho_R(1 - \alpha T + \beta S). \quad (6)$$

The coefficients of thermal and saline expansion are α and β, and ρ_R is a reference density. With the further assumption that the temperature and salinity anomalies derived from the data are perfectly coherent, the spectral energy density of the observed density signal $(\hat{\rho}_O\hat{\rho}_O^*)$, and its phase lag with respect to the observed temperature Γ are given by

$$(\hat{\rho}_O\hat{\rho}_O^*) = \rho_R^2\beta^2(\hat{S}_O\hat{S}_O^*)[1 + \chi_O^2 - 2\chi_O\cos\phi], \quad (7a)$$

$$\Gamma = \tan^{-1}\left(\frac{\sin\phi}{\cos\phi - \chi_O}\right), \quad (7b)$$

where χ_O is defined by $[(\alpha^2(\hat{T}_O\hat{T}_O^*)/\beta^2(\hat{S}_O\hat{S}_O^*)]^{1/2}$. The parameter χ_O termed the mixing ratio by Joyce *et al.* (1978), is important in the study of thermohaline finestructure. For a feature with $\chi_O = 1$, the effects of its temperature and salinity anomalies are compensating in density. The true mixing ratio χ_T is defined as $[\alpha^2(\hat{T}_T\hat{T}_T^*)/\beta^2(\hat{S}_T\hat{S}_T^*)]^{1/2}$. Values of χ_T will be compared to the observed value χ_O later in this section.

d. *Error magnitude*

Table 1 presents the error estimates of Eqs. (4) and (5) for relatively small temperature response errors using $\partial S/\partial T = 1.07$‰ °C^{-1} and $\partial S/\partial C = 1.24$‰ mmho^{-1} cm which were evaluated at $T = 2.4$°C, $C = 30.4$ mmho cm^{-1}, $P = 200$ db. The data in this table were derived using a ratio of conductivity spectral energy density to that for true temperature spectral energy density $[(\hat{C}\hat{C}^*)(\hat{T}_T\hat{T}_T)^{-1}]$ of 1.0 mmho^2 cm^{-2} °C^{-2} and $\chi_T = 0.9$. It is clear that even small response mismatches result in 1) large errors in the calculated salinity variance; 2) a large phase angle ϕ between the observed temperature and salinity data; 3) an underestimation of χ_T; 4) the observed density variance greater than the true density variance, $(\hat{\rho}_T\hat{\rho}_T^*) = \rho_R^2\beta^2(\hat{S}_T\hat{S}_T^*)[1 - \chi_T]^2$; and 5) a large phase angle Γ between the observed temperature and density.

The results in the table are not sensitive to the value used for $[(\hat{C}\hat{C}^*)(\hat{T}_T\hat{T}_T^*)^{-1}]$. A 10% change in this ratio produced less than a 1% change in the ratio of salinity variances and a 3° change in ϕ.

Methods for improving the response of the temperature channel are discussed in Section 3.

3. Lag correction techniques

a. *Introduction*

The finite response time of temperature sensors on profiling instruments introduces noise in the observed temperature data as described in Section 2. Attempts to correct the temperature data for these errors have been made in physical space and frequency space. A correction in physical space is required for accurate salinity and density data, while the correction in frequency space has importance in microstructure and dissipation measurements. Osborn and Cox (1972) expressed the thermal dissipation rate in terms of the temperature-gradient variance. This variance was estimated from an integration of temperature-gradient spectra. The total variance of the uncorrected temperature data is in error because of the amplitude-response decay of the sensor with increasing frequency. An estimate of the true variance must account for this error (Gregg, 1975).

Previous studies of sensor responses have involved the determination of the differential equations which govern the behavior of the sensor in physical space (Pingree, 1969; Lueck *et al.*, 1977). The various models have been tested by comparing the observed responses with those predicted by the differential equation in frequency space (Lueck *et al.*, 1977; Millard *et al.*, 1980; Gregg and Meagher, 1980). Once the differential equation and transfer function are known, it is a simple matter to correct temperature spectra by dividing by the amplitude response of the sensor as Osborn and Cox (1972) did. Yet, knowledge of the differential equation is not sufficient to correct the temperature data in physical space since the individual terms in the equation are not easily estimated.

For an example, consider the commonly used single-pole filter model for a temperature sensor (Gaul, 1968; Pingree, 1969)

$$\frac{dT_O}{dt} = \tau^{-1}(T_T - T_O), \tag{8}$$

where τ is a time constant. The model predicts an amplitude response with frequency of

$$R^2 = \frac{1}{(1 + \omega^2\tau^2)} \tag{9}$$

(Fofonoff *et al.*, 1974). A correction of temperature spectra thus involves multiplying each frequency estimate by $(1 + \omega^2\tau^2)$.

Fofonoff *et al.* (1974) discuss how the single-pole filter model may be used to correct temperature data in physical space. The true temperature at a given point is estimated from Eq. (8) by calculating the time rate of change of the observed temperature with a least-square linear estimation over several neighboring points. A three-point estimation boosts the temperature energy density at low frequencies but filters the high-frequency energy. Side lobes in the amplitude response are also generated by using this method of correction.

Thus, data corrected using a differential equation to model a sensor's response as above, may still be in error for two reasons. First, the differential equation may be only an approximation to the actual sensor response. Second, errors may arise in the estimation of terms in the differential equation. Knowledge of the governing differential equation is necessary to understand the dynamics of the sensor. The validity of the model, though, requires comparisons between the observed and predicted response functions. Rather than use a governing equation estimated from response observations to correct temperature data, and risk these errors, a technique was developed to use the observed response function to determine a correction filter directly.

The technique assumes that the observed temperature data may be written as a convolution of the true temperature and the response function of the sensor [Eq. (2)]. A second filter g is found to correct the data so that

$$g * f = \delta, \tag{10}$$

where δ is the delta function. From Eq. (2), the Fourier transform of g is simply the inverse of $\hat{f}$, i.e.,

$$\hat{f}^{-1} = \frac{1}{R(\omega)} \exp[-i\theta(\omega)]. \tag{11}$$

Attempts to compute g by an inverse Fourier transform of Eq. (11) are complicated by ringing in the inverse transform. The correction filter was successfully computed by selecting the set of weights whose analytic Fourier transform was a best fit to $\hat{f}^{-1}$ in a least-square sense. Although least-square fitting is not new, the selection of weights for use in the time domain, by fitting their analytic Fourier transform to the sensor response that is specified in the frequency domain, has not been done before. The method is described in detail in the Appendix.

TABLE 1. Error estimates of Eqs. (4)–(7) for relatively small temperature response errors.

R^2	θ (deg)	$\frac{(\hat{S}_O\hat{S}_O^*)}{(\hat{S}_T\hat{S}_T^*)}$	ϕ (deg)	χ_O/χ_T	$\frac{(\hat{\rho}_O\hat{\rho}_O^*)}{(\hat{\rho}_T\hat{\rho}_T^*)}$	Γ (deg)
1.0	0.0	1.0	0.0	1.0	1.0	0.0
1.0	1.0	1.01	7.1	0.99	2.5	51.4
1.0	3.0	1.12	20.5	0.95	14.6	76.3
1.0	5.0	1.32	32.4	0.87	38.7	83.3
1.01	0.0	0.94	0.0	1.04	0.42	0.0
0.995	0.0	1.03	0.0	0.98	1.4	0.0
0.990	0.0	1.06	0.0	0.97	1.8	0.0
0.99	3.0	1.18	20.0	0.92	15.3	71.3
0.99	5.0	1.39	31.6	0.84	39.4	80.1
0.90	5.0	2.00	25.7	0.67	56.8	55.1

b. Results and conclusions

The correction filter technique has been applied to data from the WHOI/NBIS CTD. Using the response function in Fig. 1, a filter was developed to correct the CTD thermistor's response errors. This filter had 31 nonzero weights which were off-centered (Fig. 3). For comparison, the three weights derived from the single-pole filter model are also displayed in Fig. 3.

Recall the amplitude response of the temperature sensor exhibits a decay with increasing frequency (Fig. 1). To remove this error, the correction filter boosts high-frequency energy. With increasing frequency, there comes a point where the filter enhances instrumental noise in the data. Therefore, the correction filter was designed to dampen energy at frequencies above this point as is shown in Fig. 3. So as not to introduce salinity noise at these frequencies, the conductivity data was also filtered above this point (Fig. 3). This filter was found using the same technique described above. The filter dampens high-frequency energy without changing the phase or low-frequency energy in the data. Finally, a pressure filter was produced to remove instrumental noise in the pressure time series (Fig. 3).

It was found that the most important correction at low frequencies was for the phase difference between temperature and conductivity, as might be expected from the response function in Fig. 1. The other corrections (amplitude, high-frequency conductivity and pressure roll-off) all produced minor additional corrections at higher frequencies. While

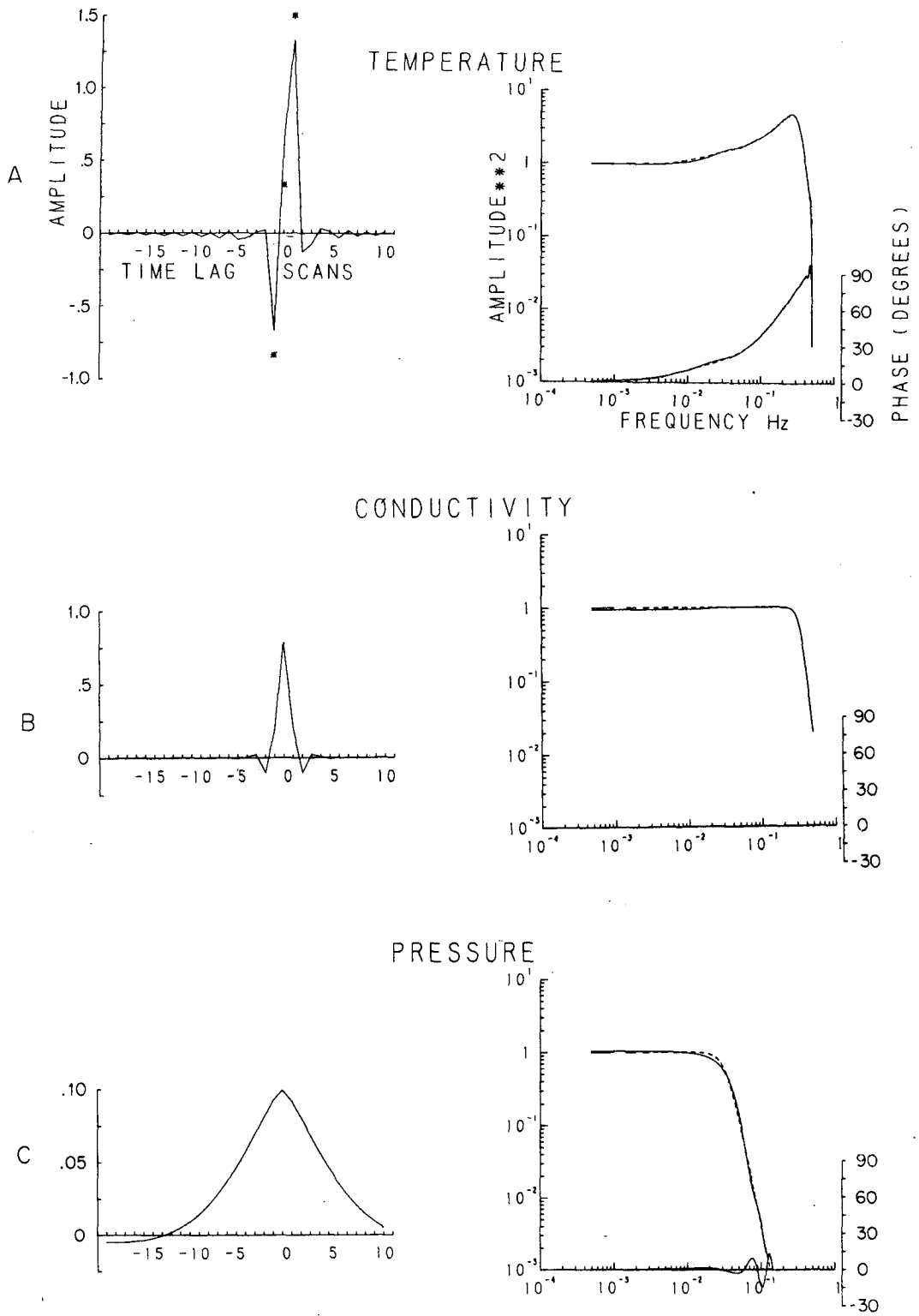

FIG. 3. The correction filters for the thermistor (A), conductivity (B) and pressure (C) data along with their response functions. The dashed curves are the true response curves used to pick the weights while the solid curves are the actual response functions of the filters shown on the left. The three starred points in Fig. 3A are the single-pole filter model weights.

the tails of the 31-point temperature filter visually appear extraneous, much of the phase information in the filter comes from them, and so cannot be neglected.

The effectiveness of the correction-filter technique described above may be evaluated in time-space and in frequency-space. Fig. 4 presents a short section of CTD lag-corrected temperature T_c and computed salinity data S_c. These data, taken in the Polar Front south of New Zealand (Bryden and Joyce, 1980), are characterized by intrusive finestructure. The vertical thermohaline gradients at intrusion interfaces are very large, as is shown in Fig. 4, and present a good test for the filtering technique. The quality of the salinity data is quite high, the small-scale noise level is low, and few spikes or overshoots are visible at the intrusion interfaces. Features on vertical scales smaller than 1 m are resolvable. For comparison, a profile of the difference between salinity computed with temperature data that were lag-corrected with the single-pole filter model S_p and S_c also appears in Fig. 4. Clearly, the noise level is much greater when using the single-pole filter and many overshoots are observable. Even more serious are areas like that between 220 and 235 db where the temperature gradient is nearly constant but the salinity calculated using the single-pole filtered temperature is too high,

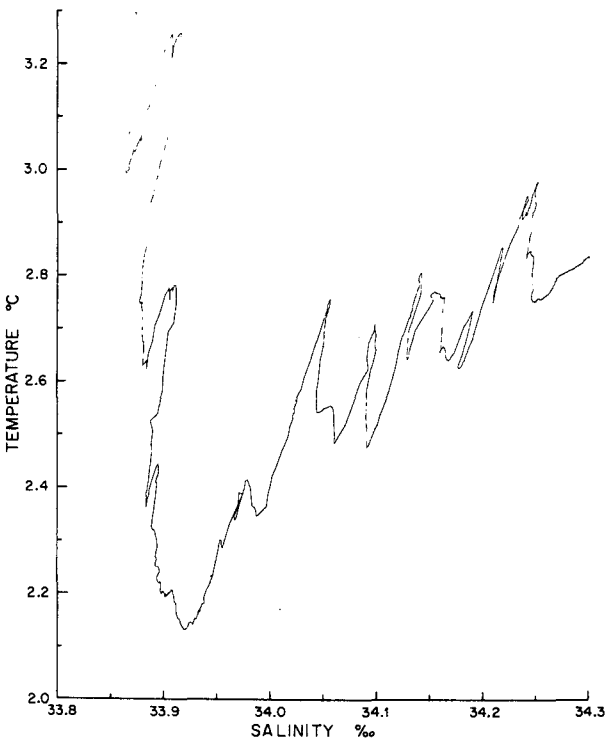

FIG. 5. A temperature salinity plot from an interleaving zone using data which were filtered to remove sensor-response mismatches.

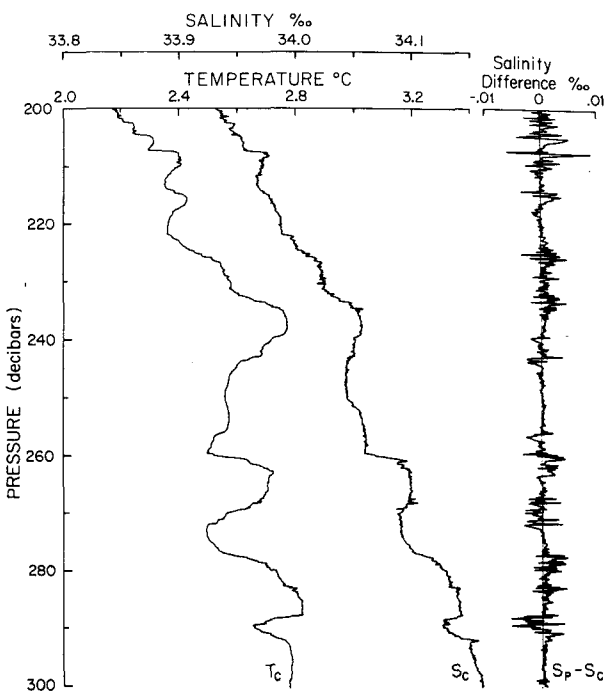

FIG. 4. Lag-corrected temperature T_c and salinity S_c data from an interleaving zone. Also shown is the difference between the salinity profile derived from temperature data which were corrected with the single pole filter model, S_p and S_c, i.e., $(S_p - S_c)$.

implying that the temperature is too low. This property of temperature data from a constant gradient region was discussed by Dantzler (1974) and will lead to many spurious density inversions.

An evaluation of the density data computed from the filtered temperature, conductivity, and pressure data may be made from a temperature-salinity (T/S) diagram (Fig. 5). Note that there are very few loops or large scale density inversions present in these data. The T/S diagram computed with the single-pole filter corrected data exhibited numerous loops, indicative of density errors.

As described in Section 2, a signature of the response mismatch between the temperature and conductivity sensors is an overestimation of salinity variance. Fig. 6 presents the average salinity-gradient spectra composited from 15 profiles in an interleaving zone using data corrected with the filtering technique and the single-pole filter model. As is seen, the salinity variance is significantly lower in the filter-corrected data on vertical scales < 40 m. The error analysis of Section 2 suggests that the temperature data corrected with the single-pole filter model have residual errors in phase of over 5° or amplitude of over 10%.

The noise level in the data can be additionally reduced by averaging the data to produce an equally-

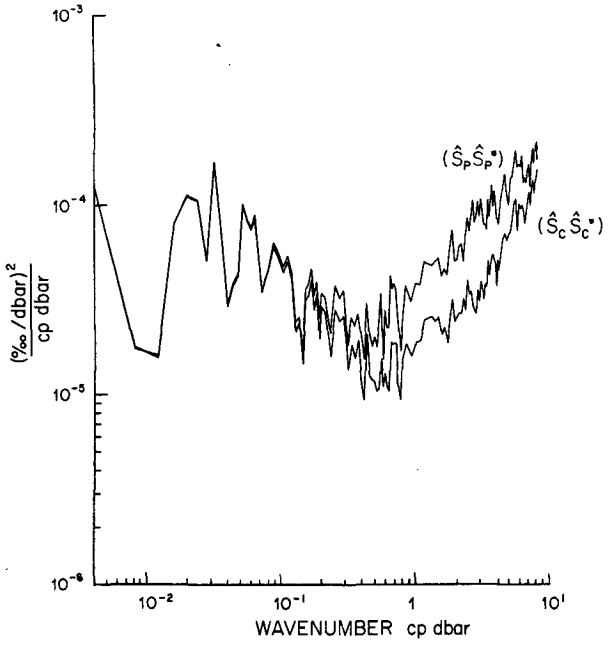

FIG. 6. Salinity gradient spectra using data which were lag corrected using the filtering technique ($\hat{S}_c\hat{S}_c^*$) and the single-pole filter model ($\hat{S}_p\hat{S}_p^*$).

spaced series in depth or pressure, as was done in Fig. 6 for both spectra. This process further acts to filter the data, applying less weight to data when the instrument is descending slowly, and neglecting data when the instrument reverses direction, as occasionally happens when lowering in heavy seas (Pingree, 1971). This points out the major error involved in the filtering technique. The method assumes the response functions of the sensors are constant. In fact, the response functions of most temperature and conductivity sensors are lowering-rate dependent, and the majority of the profiling instruments are ship-lowered and so subject to variations in the lowering rate due to ship roll. The filtering technique described here corrects only for the average responses. Errors should be expected in data which have highly variable package-descent rates. With accurate knowledge of the sensor responses as functions of lowering rate it should be possible to develop correction filters which are lowering-rate dependent to treat these data.

The technique described here has been applied to correct response errors in both the thermistor and the platinum thermometer on the WHOI/Brown CTD with excellent results. The method also may be used on data from standard CTD's that combine the platinum thermometer and thermistor signals, or from any other instrument once the response function for the data is known.

Acknowledgments. The authors would like to thank D. Georgi for numerous helpful suggestions, and to acknowledge the support of National Science Foundation Grant OCE77-28355 to the Woods Hole Oceanographic Institution.

APPENDIX

Determination of Correction Filters

In time space let an approximation to the correction filter g consist of a set of $2n$ weights

$$W(r\Delta),$$

$$\{r = -n, -n+1, \ldots, 0, 1, 2, \ldots n-1\}, \quad \text{(A1)}$$

where Δ is the sampling period of the data. If all the $2n$ weights are allowed to be nonzero, with $2n$ equal to the number of frequency estimates in the representation of the response function, it is possible to determine the weights which fit the inverse of the response function exactly. Because of the large number of data points involved, this is impractical. However, by setting most of the weights to zero it becomes feasible to find the best values in the least-squares sense for these weights to match the inverse of the response function.

Let p be the index of the first of a series of l consecutive nonzero weights. From (A1)

$$W(r\Delta) = \{0, 0, \ldots, w(p), w(p+1), \ldots, w(p+l-1), \ldots, 0, 0\},$$
$$-n < p < p + l - 1 < n - 1. \quad \text{(A2)}$$

$W(r\Delta)$ may be expanded in a Fourier series

$$W(r\Delta) = A_0 + 2\sum_{m=1}^{n-1}\left[A_m \cos\left(\frac{2\pi mr}{N}\right) + B_m \sin\left(\frac{2\pi mr}{N}\right)\right] + A_n \cos\left(\frac{2\pi nr}{N}\right), \quad \text{(A3)}$$

where

$$N = 2n,$$

$$A_0 = \frac{1}{N}\sum_{r=p}^{p+l-1} W(r\Delta),$$

$$A_m = \frac{1}{N}\sum_{r=p}^{p+l-1} W(r\Delta)\cos\left(\frac{2\pi mr}{N}\right),$$

$$B_m = \frac{1}{N}\sum_{r=p}^{p+l-1} W(r\Delta)\sin\left(\frac{2\pi mr}{N}\right),$$

$$A_n = \frac{1}{N}\sum_{r=p}^{p+l-1} W(r\Delta)\cos\pi r.$$

As shown, the summations are only over the nonzero terms.

In frequency space, the Fourier transform of the weights is given by

$$\hat{W}(r\Delta) = A_m + iB_m, \quad m = 0, 1, 2, \ldots, n, \quad \text{(A4)}$$

while $\hat{f}^{-1}$ may be written as

$$\hat{f}^{-1} = C_m + iD_m, \quad m = 0, 1, 2, \ldots, n. \quad \text{(A5)}$$

The values of the nonzero weights are selected to minimize

$$\epsilon = \sum_{m=0}^{n} [(A_m - C_m)^2 + (B_m - D_m)^2]. \quad \text{(A6)}$$

Substituting from (A3) and letting $\Delta = 1$ gives

$$\epsilon = \sum_{m=1}^{n-1} \left\{ \left[\frac{1}{N} \sum_{r=p}^{p+l-1} W(r) \cos\left(\frac{2\pi mr}{N}\right) - C_m \right]^2 + \left[\frac{1}{N} \sum_{r=p}^{p+l-1} W(r) \sin\left(\frac{2\pi mr}{N}\right) - D_m \right]^2 \right\} + \left[\frac{1}{N} \sum_{r=p}^{p+l-1} W(r) - C_0 \right]^2 + \left[\frac{1}{N} \sum_{r=p}^{p+l-1} W(r) \cos\pi r - C_n \right]^2 . \quad \text{(A7)}$$

To determine $W(r)$ by a least-square technique, the derivative of ϵ with respect to each of the weights is set equal to zero. This yields a set of l linear equations of the form

$$\sum_{m=1}^{n-1} \left[\cos\left(\frac{2\pi mk}{N}\right) \sum_{r=p}^{p+l-1} W(r) \cos\left(\frac{2\pi mr}{N}\right) + \sin\left(\frac{2\pi mk}{N}\right) \sum_{r=p}^{p+l-1} W(r) \sin\left(\frac{2\pi mr}{N}\right) \right] + \sum_{r=p}^{p+l-1} W(r) + \cos\pi k \sum_{r=p}^{p+l-1} W(r) \cos\pi r = \sum_{m=1}^{n-1} N \left[\cos\left(\frac{2\pi mk}{N}\right) C_m + \sin\left(\frac{2\pi mk}{N}\right) D_m \right] + NC_0 + NC_n \cos\pi k,$$

$$k = p, p + 1, \ldots, p + l - 1. \quad \text{(A8)}$$

As in all least-square problems, this set of the "normal equations" may be written in the form

$$\mathbf{A}^T\mathbf{A}\bar{\mathbf{W}} = A^T\mathbf{B}, \quad \text{(A9)}$$

where $\mathbf{A}$ is an $l \times N$ matrix and $\mathbf{A}^T$ is its transpose. $\bar{\mathbf{W}}$ is a vector containing the l unknown $W(r)$'s and $\mathbf{B}$ is a vector containing the $n + 1$ C_m's and $n - 1$ D_m's describing the response function. The terms in the $\mathbf{A}$ matrix appear as below:

$$\mathbf{A} = \begin{matrix} H(1,p) & H(1,p+1) & \cdots & H(1,p+l-1) \\ H(2,p) & H(2,p+1) & \cdots & H(2,p+l-1) \\ \vdots & & & \\ H(n-1,p) & H(n-1,p+1) & \cdots & H(n-1,p+l-1) \\ S(1,p) & S(1,p+1) & \cdots & S(n-1,p+l-1) \\ \vdots & & & \\ S(n-1,p) & S(n-1,p+1) & \cdots & S(n-1,p+l-1) \\ N & N & \cdots & N \\ Q(p) & Q(p+1) & \cdots & Q(p+l-1) \end{matrix} \quad \text{(A10)}$$

where $H(m,k) = \cos(2\pi mk/N)$, $S(m,k) = \sin(2\pi mk/N)$ and $Q(k) = \cos\pi k$.

The terms in the $\mathbf{B}$ matrix take the form

$$\mathbf{B} = \begin{matrix} C_1 \\ C_2 \\ \vdots \\ C_{n-1} \\ D_1 \\ D_2 \\ \vdots \\ D_{n-1} \\ C_0 \\ C_n \end{matrix}$$

which describe the spectral response of the sensor being corrected.

To determine the weights, the matrix $\mathbf{A}^T\mathbf{A}$ is inverted since from (A9)

$$\bar{\mathbf{W}} = (\mathbf{A}^T\mathbf{A})^{-1}\mathbf{A}^T\mathbf{B}. \quad \text{(A11)}$$

Using the above description of the $\mathbf{A}$ matrix, it is possible to write down an analytic expression for the terms in $\mathbf{A}^T\mathbf{A}$ so that the largest matrix stored in the computer is $l \times l$ with l typically <100. The matrix $\mathbf{A}^T\mathbf{A}$ is also symmetric so that only half its terms need be stored.

In practice there are two parameters which can be varied to adjust the response of the filter; l the number of weights in the filter, and p, the position of the filter with respect to the center point (i.e., is it centered, forward, backward, or somewhere in between). A trial and error method was used to find the combination which produced the best results.

Occasionally, one is only interested in data in a certain frequency band. The correction filter can be tuned to emphasize the fit in that band using a weighted least-square fit. The filters shown in Fig. 3 were weighted toward high frequencies.

REFERENCES

Brown, N. L., 1963: A proposed *in situ* salinity sensing system. *Mar. Sci. Instrum.*, **2**, 19–24.

——, 1974: A precision CTD microprofiler. *Ocean 74, 1974 IEEE Int. Conf. Engng. Ocean Envir. Rec.*, 270–278.

Bryden, H. L., and T. M. Joyce, 1980: Studies of eddies and interleaving water masses east and south of New Zealand. *Antarct. J. U.S.* (in press).

Dantzler, H. L., Jr., 1974: Dynamic salinity calibrations of continuous salinity/temperature/depth data. *Deep-Sea Res.*, **21**, 675–682.

Fofonoff, N. P., S. P. Hayes and R. C. Millard, 1974: WHOI/Brown CTD microprofiler: methods of calibration and data handling. Woods Hole Oceanographic Institution Tech. Rep. WHOI-74-89, 64 pp.

Gaul, R. D., 1968: Performance analysis of a salinity/temperature depth system. *IEEE Trans. Geosci. Electron.*, **GE-6**, 185–189.

Gregg, M. C., 1975: Microstructure and Intrusions in the California Current. *J. Phys. Oceanogr.*, **5**, 253–278.

——, and C. S. Cox, 1971: Measurement of the oceanic microstructure of temperature and electrical conductivity. *Deep-Sea Res.*, **18**, 925–934.

——, and T. B. Meagher, 1980: The dynamic response of glass-rod thermistors. Submitted to *J. Phys. Oceanogr.*

Hamon, B. V., and N. L. Brown, 1958: A temperature-chlorinity-depth recorder for use at sea. *J. Sci. Instrum.*, **35**, 452–458.

Joyce, T. M., W. Zenk and J. M. Toole, 1978: The anatomy of the Antarctic Polar Front in the Drake Passage. *J. Geophys. Res.*, **83**, 6093–6113.

Kroebel, W., 1973: Die Kieler Multimeeressonde. *"Meteor" Forschungsergeh*, Reihe A, No. 12, 53–67.

Lueck, R. G., D. Hertzman and T. R. Osborn, 1977: The spectral response of thermistors. *Deep-Sea Res.*, **24**, 951–970.

Millard, R., J. Toole and M. Swartz, 1980: A fast responding temperature measurement system for CTD applications. *Ocean Eng.*, **7** (in press).

Osborn, T. R., and C. S. Cox, 1972: Oceanic fine structure. *Geophys. Fluid Dyn.*, **3**, 321–345.

Pingree, R. D., 1969: Small-scale structure of temperature and salinity near station Cavall. *Deep-Sea Res.*, **16**, 275–295.

——, 1971: Regularly spaced instrumental temperature and salinity structures. *Deep-Sea Res.*, **18**, 841–844.

Scarlet, R. I., 1975: A data processing method for salinity, temperature, depth profiles. *Deep-Sea Res.*, **22**, 509–515.